Supporting information

Enhanced Sodium Ion Storage in MnO_2 through Asymmetric Orbital Hybridizations Induced by Spin-Paired Ion Doping

Jinrui Wang[a,1], Xia Liu[a,1], Zishan Hou[a], Shiyu Wang[a], Shuyun Yao[a], Xueying Gao[a], Yuanming Liu[a], Kaiqi Nie[c], Jiangzhou Xie[b,*], Zhiyu Yang[a,*], Yi-Ming Yan[a,*]

[1] These authors contributed equally to this work.

[a] State Key Laboratory of Organic-Inorganic Composites, Beijing Advanced Innovation Center for Soft Matter Science and Engineering, Beijing University of Chemical Technology, Beijing, 100029, People's Republic of China

[b] School of Mechanical and Manufacturing Engineering, University of New South Wales, Sydney, New South Wales 2052, Australia

[c] Institute of High Energy Physics, Chinese Academy of Sciences, Beijing 100049, People's Republic of China

Corresponding authors.

E-mail: yanym22@mail.buct.edu.cn;

yangzhiyu@mail.buct.edu.cn;

jiangzhou.xie@unsw.edu.au

Experimental Procedures

Chemicals and reagents

$Mn(NO_3)_2$ and Tetramethylammonium hydroxide (TMA·OH) were obtained from Shanghai Macklin Biochemical Co., Ltd. $SnCl_4·5H_2O$ was obtained from Innochem. H_2O_2 was purchased from Beijing Chemical Works. Anhydrous (Na_2SO_4) was purchased from Beijing Tong Guang Fine Chemicals Company. All reagents were used as received without further purification. And all solutions were prepared using ultrapure water (resistance = 18.2 MΩ cm).

Characterization of the sample

Microstructure were studied using scanning electron microscopy (SEM, FEI Quanta 200) at 20 kV, transmission electron microscopy (TEM; FEI Tecnai G2 20) and HRTEM (JEOL, JEM-2100, 200 kV). The electronic structure and compositional information on the samples were investigated by X-ray photoelectron spectroscopy (XPS, ESCALAB 250). The band gap of the materials were determined by UV-vis adsorption spectroscopy (Varian Cary 6000i) in the wavelength range of 250-800nm. JEOLJESFA200 EPR spectrometer was used to obtain the electron paramagnetic resonance (EPR) spectra, and operating parameters were 140K, 9064 MHz, 0.998 mW, X-band. The soft-XAS measurements were carried out in total electron yield mode under ultra-high vacuum at beamline 4B9B of Beijing Synchrotron Radiation Facility of the Institute of High Energy Physics, Chinese Academy of Sciences. Au $4f_{7/2}$ core level spectra were recorded for the photon energy calibration, and the energy resolution is better than 0.2 eV at room temperature. The electrochemical operando Cell (EC-RAIR-H) is supplied by Beijing Science Star technology Co. Ltd. The Raman spectrum was recorded on a HORIBA Raman microscope with a laser wavelength of 532 nm (LabRAM Aramis, HORIBA Jobin Yvon S.A.S, France) for surface characterization. Raman spectra of the sample (one spectrum per 30 s) were captured while a cyclic voltammetry test at a scan rate of 2 mV s^{-1} simultaneously.

Electrochemical measurements

Working electrode was prepared by traditional slurry-coating method. 80 wt% active material, 10 wt% acetylene black and 10 wt% polytetrafluoroethylene (PTFE) was mixed and coated onto carbon cloth with an area of 1 cm^2. The electrode was then heated at 60 ℃ for 2 hours to evaporate the solvent and used as working electrode. The negative electrode was prepared by mixing active carbon, acetylene black and PTFE with a mass ratio of 8:1:1. Electrochemical measurements were conducted in a general three-electrode configuration in 1.0

M Na_2SO_4 aqueous electrolyte with Ag/AgCl and a Pt foil as reference electrode and counter electrode, respectively. Cyclic voltammetry (CV) and galvanostatic charge discharge (GCD) experiments were performed to determine the electrochemical properties of the electrodes in a potential window of -0.1 to 0.9 V. All the operating current densities were calculated based on the mass of the active materials Electrochemical impedance spectroscopy (EIS) measurements were carried out by applying an AC voltage with 5 mV amplitude in a frequency range from 0.01 Hz to 100 kHz at open potential.

The specific capacitance C (F g^{-1}) was calculated based on the GCD curves according to equation [1] :

$$C = \frac{I \times \Delta t}{m \times V} \quad \text{(S1)}$$

where I (A) and Δt (s) are the discharge current and time, respectively, m (g) represents of the active material's loading mass and V refers to the charge/discharge potential window.

Sodium diffusion coefficient calculation

The diffusion coefficient of Na^+ (D_{Na^+}) can be obtained from the low frequency line according to the equation [2]:

$$D_{Na+} = 0.5(RT/AF^2C\sigma)^2 \quad \text{(S2)}$$

where R, T, F, A, and C are the gas constant, the absolute temperature, the Faraday's constant, the apparent area of the electrode, and the molar concentration of Na^+, respectively. σ is the Warburg factor following Equation:

$$Z' = Re + Rct + \sigma\omega^{-\frac{1}{2}} \quad \text{(S3)}$$

where R_e is the resistance between the electrolyte and electrode, and R_{ct} is the charge transfer resistance. Thus, the slopes of the plot of Z' vs $\omega^{-1/2}$ can used to obtain the values of σ.

Kinetic calculation

Capacitance contribution can be qualitatively analysed according to CV curve, as shown below [3]:

$$i = av^b \quad \text{(S4)}$$

where i and v are the current density and the potential scan rate, respectively, α is a constant and b is a tunable parameter with a value of 0.5-1.0. When the value of b is close to 1.0, the reaction process is dominated by surface capacitance; when the value of b is close to 0.5, the reaction process is dominated by diffusion control.

The contribution of capacitance and diffusion limit to the total capacitance is further quantified [4].

$$i(V) = k_1 v + k_2 v^{1/2} \quad \text{(S5)}$$

where k_1 and k_2 represent capacitive and diffusion contributions, respectively. By determining both k_1 and k_2, it is thus possible to distinguish the fraction of the current arising from Na^+ insertion and that from capacitive processes at specific potentials.

Supercapacitor devices measurements

Supercapacitor Devices Measurements: Asymmetric supercapacitor (ASC) device was fabricated by employing Sn-MnO_2 and AC as cathode and anode, respectively. Two electrodes were separated by glassy fibrous separator in 1 M Na_2SO_4 aqueous electrolyte. Cyclic voltammetry (CV) and galvanostatic charge/discharge (GCD) measurements were performed in a potential window of -0.1 to 0.9 V.

The energy density (E, Wh kg^{-1}) of the ASC is calculated according to S6 [5]:

$$E = \frac{C \times V^2}{2} \times \frac{1000}{3600} \quad \text{(S6)}$$

The power density (P, W kg^{-1}) of the ASC is calculated according to S7 [6]:

$$P = \frac{E \times 3600}{t} \quad \text{(S7)}$$

where t (s) is discharge time.

DFT Methods

We have employed the Vienna Ab initio Simulation Package (VASP) to perform all density functional theory (DFT) calculations within spin-polarized frame. The elemental core and valence electrons were represented by the projector augmented wave (PAW) method and plane-wave basis functions with a cutoff energy of 520 eV. Generalized gradient approximation with the Perdew-Burke-Ernzerhof (GGA-PBE) exchange-correlation functional was employed in all the calculations. The DFT-D3 empirical correction method was employed to describe van der Waals interactions. Geometry optimizations were performed with the force convergency smaller than 0.07 eV/Å. Monkhorst-Pack k-points of 1×1×1 was applied for all the calculations. To overcome this shortcoming, the GGA+U approach was used with U-J = 3.9 eV for the Mn atoms.

Supporting figures

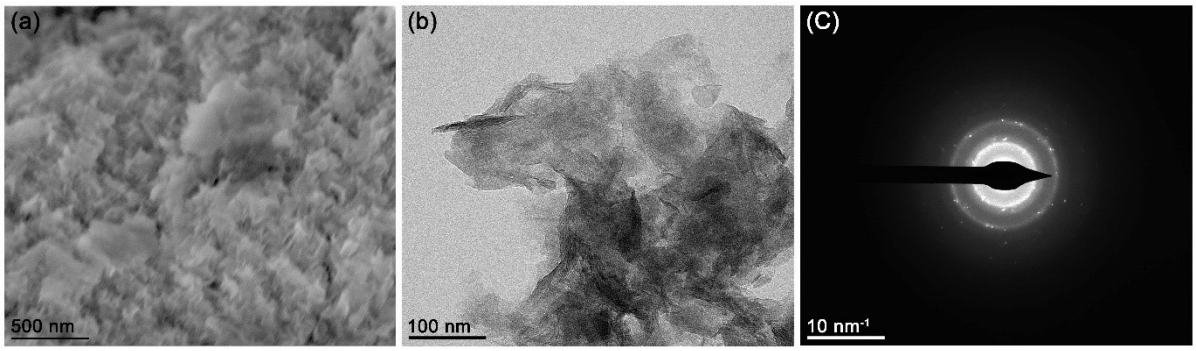

Fig. S1 (a) SEM image and (b) TEM image of MnO_2, (c) SAED image of MnO_2.

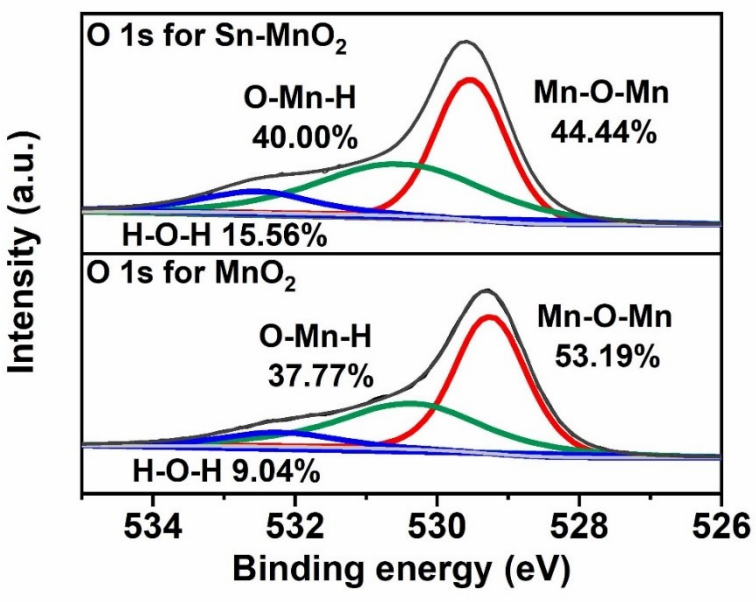

Fig. S2 XPS spectra: O 1s of Sn-MnO_2 and MnO_2.

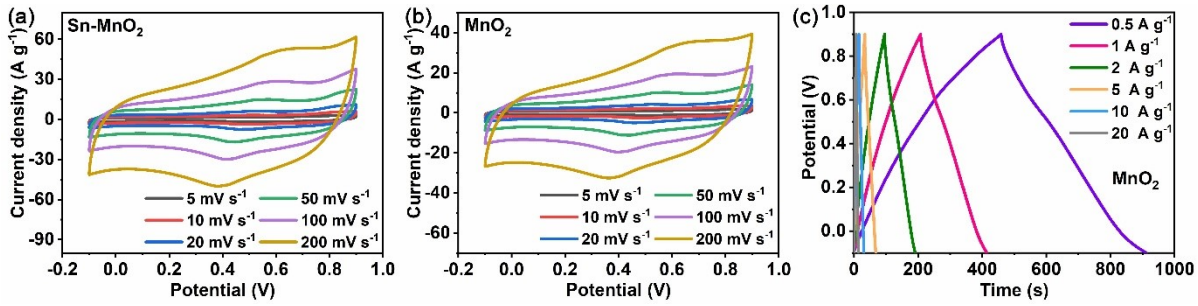

Fig. S3 (a, b) CV curves of Sn-MnO_2 and MnO_2 samples at different scan rates from 5-200 mV s^{-1}. (c) GCD curves at different current densities of MnO_2 sample.

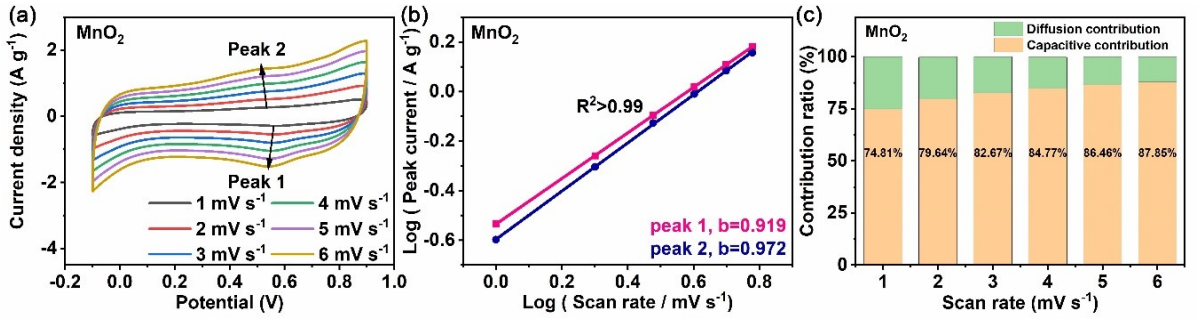

Fig. S4 (a) CV curves of MnO_2 at different scan from 1-6 mV s^{-1}. (b) The linear fitting curves of log (i) versus log (v) according to the CV results in (a). (c) Diffusion contributions and capacitive contributions of MnO_2.

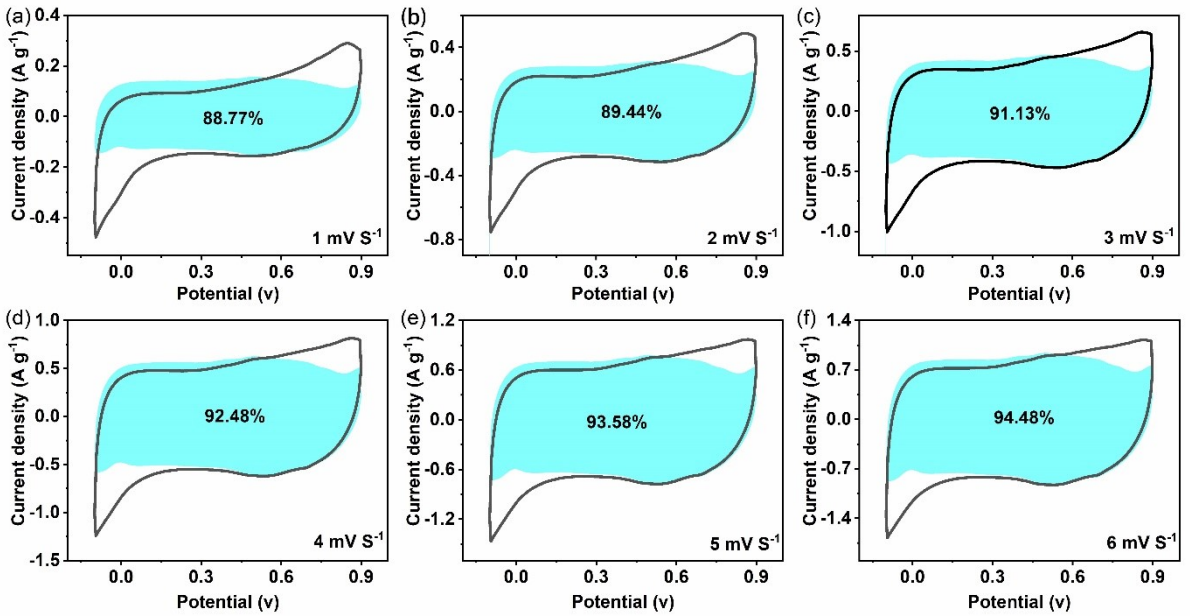

Fig. S5 Pseudocapacitive fraction (shown by the shaded area) calculated at a scan rate of 1-6 mV s^{-1} from CV curves at different scan rates of (a, b, c, d, e, f) Sn-MnO_2 electrode.

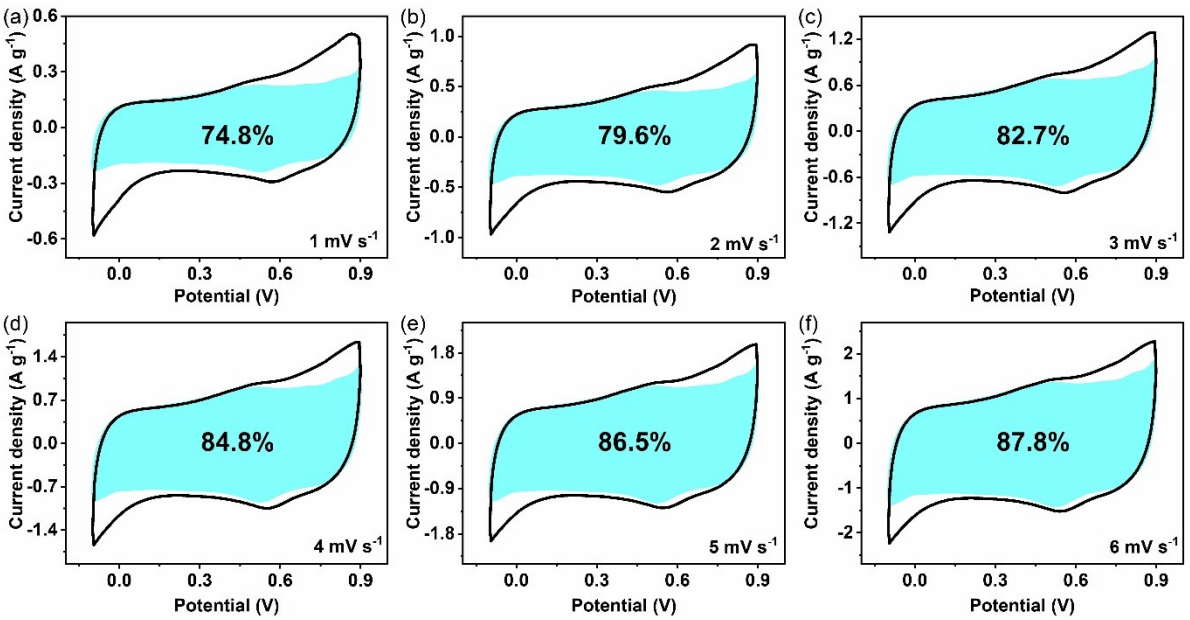

Fig. S6 Pseudocapacitive fraction (shown by the shaded area) calculated at a scan rate of 1-6 mV s^{-1} from CV curves at different scan rates of (a, b, c, d, e, f) MnO_2 electrode.

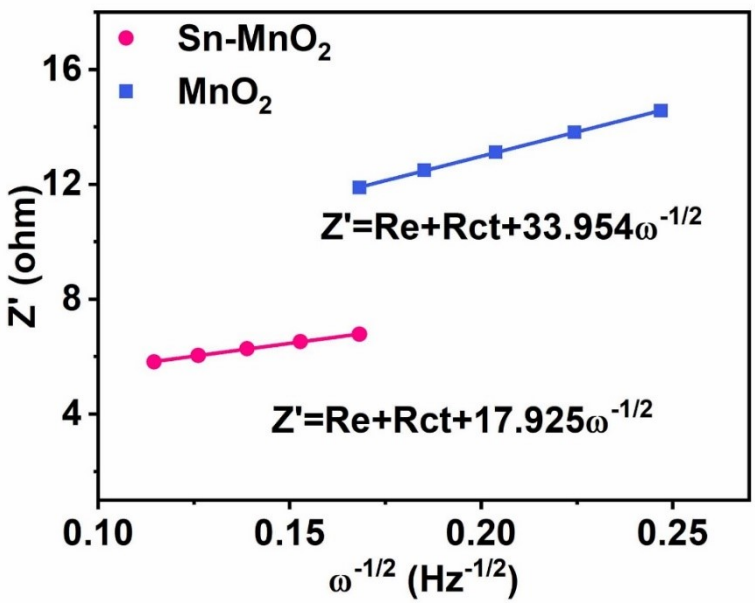

Fig. S7 Diagram of Z' and $\omega^{-1/2}$ in the low frequency zone obtained from EIS measurement and the calculated diffusion coefficient of Sn-MnO_2 and MnO_2.

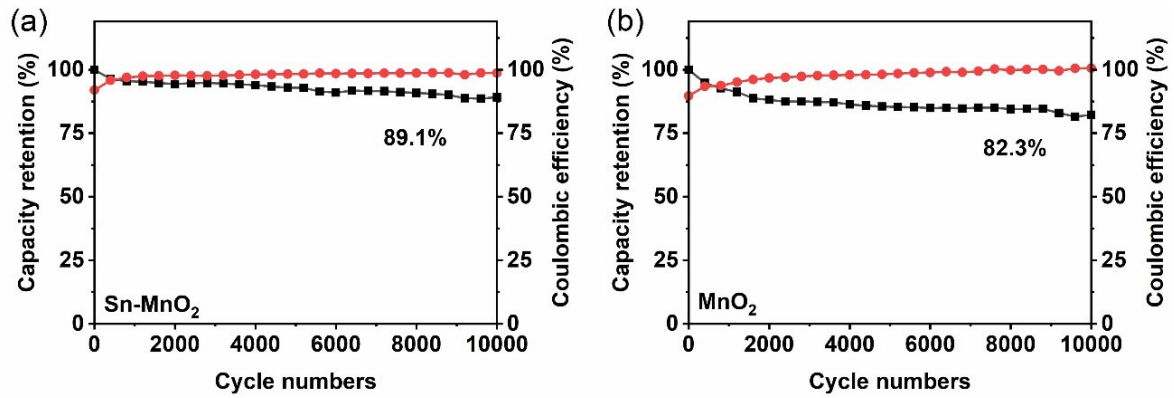

Fig. S8 (a, b) Cycling stability of Sn-MnO_2 electrode and MnO_2 electrode at a current density of 1 A g^{-1}.

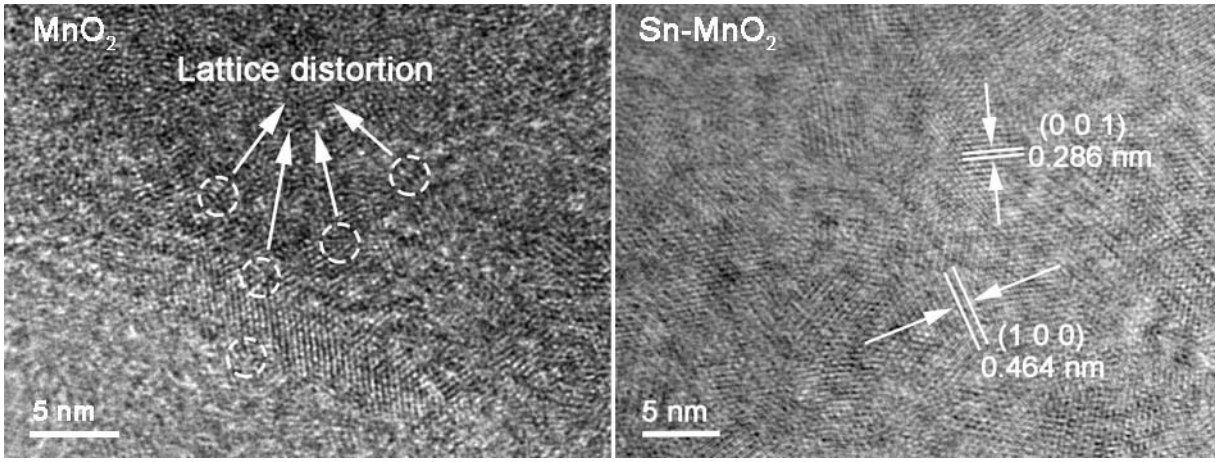

Fig. S9. HRTEM images of cycled MnO_2 and Sn-MnO_2 cathode materials.

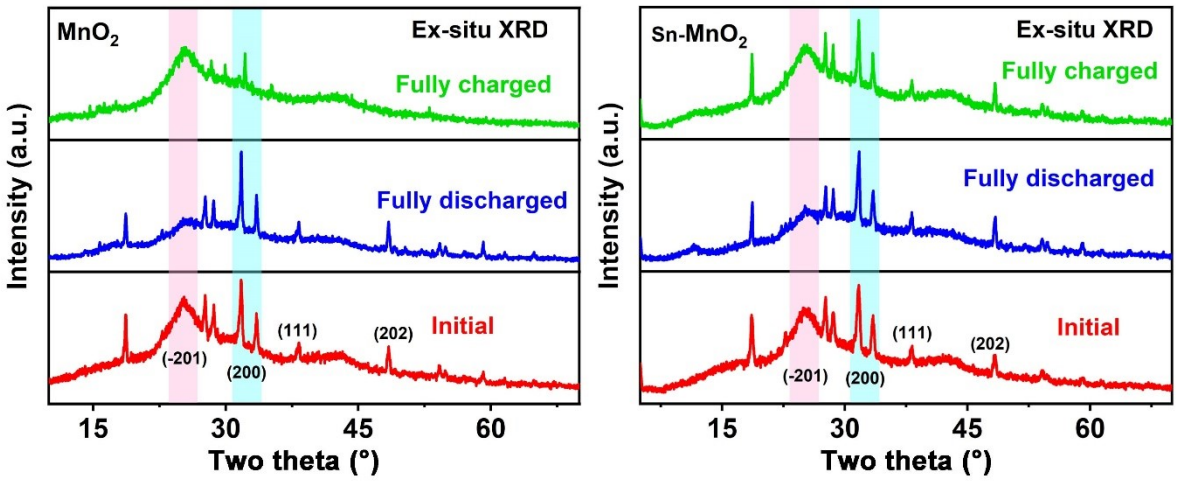

Fig. S10. Ex-situ XRD patterns of MnO_2 and Sn-MnO_2.

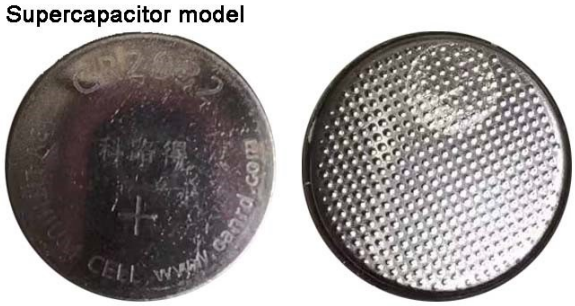

Fig. S11. The assembled prototype of the supercapacitor.

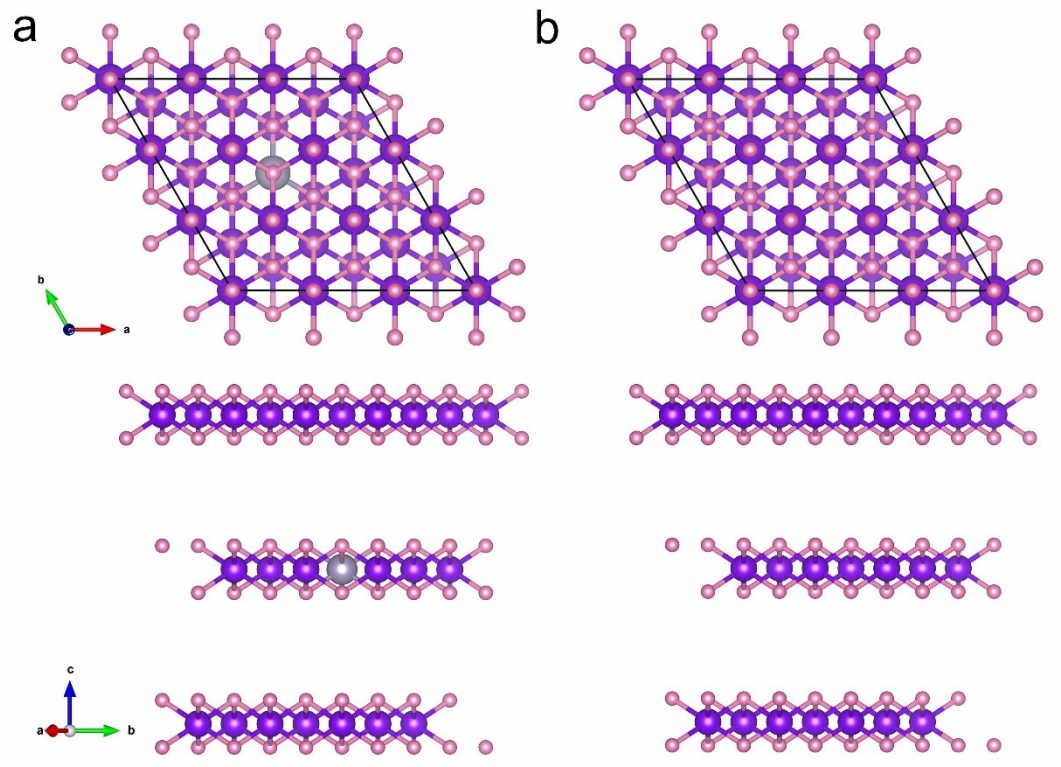

Fig. S12 The top view (above) and side view (below) of optimized structure for (a) undoped Sn-MnO_2 and (b) MnO_2. Color codes: Mn, purple; O, pink; Sn, grey, respectively.

References

1. M. Jana, P. Samanta, N. C. Murmu and T. Kuila, *Chem. Eng. J.*, 2017, **330**, 914-925.
2. S. Wang, R. Zhao, S. Yao, B. Li, R. Liu, L. Hu, A. Zhang, R. Yang, X. Liu, Z. Fu, D. Wang, Z. Yang and Y.-M. Yan, *Journal of Materials Chemistry A*, 2021, **9**, 23506-23514.
3. S. Wang, L. Li, Y. Shao, L. Zhang, Y. Li, Y. Wu and X. Hao, *Adv Mater*, 2019, **31**, e1806088.
4. C. Zhao, C. Yu, M. Zhang, H. Huang, S. Li, X. Han, Z. Liu, J. Yang, W. Xiao, J. Liang, X. Sun and J. Qiu, *Adv. Energy Mater.*, 2017, **7**, 1602880.
5. A. Zhang, R. Gao, L. Hu, X. Zang, R. Yang, S. Wang, S. Yao, Z. Yang, H. Hao and Y.-M. Yan, *Chemical Engineering Journal*, 2021, **417**.
6. Y. Bai, B. Shen, S. Zhang, Z. Zhu, S. Sun, J. Gao, B. Li, Y. Wang, R. Zhang and F. Wei, *Adv. Mater.*, 2019, **31**, 1800680.